agriculture

MDPI

Article

Design and Testing of a Branched Air-Chamber Type Pneumatic Seed Metering Device for Rice

Xiantao Zha [1,2], Lin Chen [1,2], Dongquan Chen [1,2], Yupeng He [1,2] and Ranbing Yang [1,2,*]

[1] School of Mechanical and Electrical Engineering, Hainan University, Haikou 570228, China; zhaxt@hainanu.edu.cn (X.Z.); 22220951360007@hainanu.edu.cn (L.C.); donnchen@hainanu.edu.cn (D.C.); 22210802000010@hainanu.edu.cn (Y.H.)

[2] Key Laboratory of Tropical Intelligent Agricultural Equipment, Ministry of Agriculture and Rural Affairs, Haikou 570228, China

* Correspondence: yangranbing@hainanu.edu.cn

Abstract: To meet the diverse seeding requirements of super hybrid rice, common hybrid rice, and conventional rice—which vary from 1 to 3 seeds, 2 to 4 seeds, and 5 to 8 seeds per hole, respectively—this study developed a branched air-chamber type pneumatic seed metering device for rice. The device utilizes an air chamber control board to manage the branched air chamber casing, enabling precise adjustments to the seeding quantity. This study presents a theoretical analysis of the seed metering device's operation and its critical components. Structural parameter optimization was conducted using Ansys-Fluent (2021 R1) software, followed by multi-objective optimization of operational parameters through bench testing. Simulation results indicated that optimal vacuum pressure in the seed metering disc pores reached a maximum of 857 Pa with a chamber depth of 22 mm, an angle of 100°, and a cavity depth of 25 mm, achieving a minimal coefficient of variation of 0.86%. Bench test results showed that for seeding targets of 1 to 3 rice seeds per hole, the optimal operational parameters were: two openings, a working vacuum of 1355 Pa, and a rotor speed of 32.78 r/min, resulting in a missed seeding rate of 4.70%, a qualification rate of 85.81%, and a re-seeding rate of 9.49%. For targets of 2 to 4 seeds per hole, the best parameters included three openings, a working vacuum of 1357 Pa, and a speed of 32.87 r/min, with a missed seeding rate of 4.60%, a qualification rate of 85.59%, and a re-seeding rate of 9.81%. For 5 to 8 seeds per hole, optimal parameters were six openings, a vacuum of 1339 Pa, and a rotor speed of 31.07 r/min, yielding a missed seeding rate of 4.09%, a qualification rate of 87.27%, and a re-seeding rate of 8.64%. These findings demonstrate that the branched air-chamber type pneumatic seed metering device effectively meets the varied direct seeding requirements of rice, enhancing the adaptability of pneumatic seed metering devices to different seeding quantities in rice and potentially informing the design of pneumatic seeders for other crops.

Keywords: rice; precision drilling; adjustable seeding rate; pneumatic seed metering device; fluid simulation

Citation: Zha, X.; Chen, L.; Chen, D.; He, Y.; Yang, R. Design and Testing of a Branched Air-Chamber Type Pneumatic Seed Metering Device for Rice. *Agriculture* **2024**, *14*, 1934. https://doi.org/10.3390/agriculture14111934

Academic Editor: John M. Fielke

Received: 8 October 2024
Revised: 26 October 2024
Accepted: 29 October 2024
Published: 30 October 2024

1. Introduction

Rice ranks among the three major cultivated cereal crops worldwide, alongside wheat and maize, and serves as a staple food for over three billion people globally [1]. Mechanical direct seeding of rice is recognized as an efficient and simplified planting method [2–5]. In Western countries, aerial seeding predominates, whereas in China, orderly mechanical direct seeding is more commonly adopted [6]. This method offers distinct advantages over mechanical transplanting, such as simplicity of the planting process and reduced rice growth periods. There are significant differences in seeding rates between hybrid and conventional rice when direct seeding techniques are employed [7]; with the ongoing advancements in hybrid rice seed production, seeding rates for super hybrid rice are now as low as 1 to 3 seeds per hill [8,9], compared to 2 to 4 seeds per hill for standard

hybrid rice [10,11], and 5 to 8 seeds per hill for conventional rice [12]. Consequently, precise adjustment technologies and equipment have become crucial for the application of mechanized direct seeding modes in rice cultivation.

The key component of precise hill-seeding technology is the seed metering device, whose performance directly impacts the quality of seeding [13,14]. Mechanical metering devices typically adjust seed rates by altering the size of the holes. However, rice seeds, being elongated ellipsoids, tend to stack disorderly in the fill zone, resulting in a random number of seeds filling the holes within a certain range, thus leading to low adjustment precision and complicated processes [15,16]. Pneumatic seed metering devices have become widely used due to their high adaptability to seed shapes, low damage rates, and suitability for high-speed seeding operations [17,18]. In response, scholars have focused on optimizing the structure of pneumatic seed metering devices for precise rice seeding. Wang et al. introduced a method for infinitely adjustable seeding rates, using Bluetooth to control the rotation of an internal stepper motor within the seed metering wheel, thereby changing the angle between the internal and external wheels to alter the hole volume and achieve infinite seed rate adjustment [19]. Zang et al. developed a single-grain pneumatic metering device for hybrid rice with rectangular suction holes, determining optimal parameters for the suction holes, working negative pressure, and operational speed through gas–solid coupling simulations and bench tests [20]. Xing et al. conducted an optimization study on a pneumatic seed metering device for rice, using a combination of theoretical analysis and bench testing. They determined the optimal combinations of parameters such as the negative pressure in the suction chamber, the rotational speed of the seed metering disc, and the number of suction holes on the seed metering disc under various seeding volumes [21,22]. To meet the precision seeding requirements of both hybrid and conventional rice, Zhang et al. and his team developed a dual-chamber, side-filling seed metering device. This device features a dual-chamber structure that allows for adjustable seed dispensing rates, accommodating both hybrid and conventional rice [23]. Zhang et al. proposed a combined type-hole seed metering device consisting of a type-hole wheel casing, type-hole wheel, and an adjustment mechanism. Their experiments clarified the type-hole volumes needed to adapt to different seeding rates for hybrid and conventional rice [24]. Zhang et al. introduced a mechanical guidance filling seed metering device, which adjusts the rice seed dispensing rate by switching the size of the type-holes and adjusting the effective length of the seed entry holes [25].

In summary, addressing the poor adaptability of existing pneumatic seed metering devices to varying rice seed volumes, this study has developed a branched air-chamber type pneumatic precise seed metering device for rice. By adjusting the openings in the branched air chamber casing, this device precisely controls the seed dispensing rate to meet the diverse needs of super hybrid rice, ordinary hybrid rice, and conventional rice for direct seeding. The optimization of structural parameters and operating parameters of key components was conducted through theoretical analysis, Ansys-Fluent simulation tests, bench testing, and multi-combination optimization, with the optimized results validated through bench testing.

2. Materials and Methods

As depicted in Figure 1, the study was divided into two modules, which build upon each other. Module 1: Design of the branched air chamber casing. Based on analysis and specific requirements, the evaluation indicators and factors for the tests were determined, followed by fluid domain simulation for single-factor and orthogonal tests. The model of the branched air chamber casing was then selected based on the test results. Module 2: Optimization of operating parameters and performance testing of the seed metering device. Using the branched air chamber casing determined in Module 1 as a key component of the seed metering device, initial bench test designs were created to establish evaluation indicators and factors, followed by single-factor and orthogonal tests. The data from these

tests were then optimized, with the final optimized results subjected to validation testing and performance evaluation.

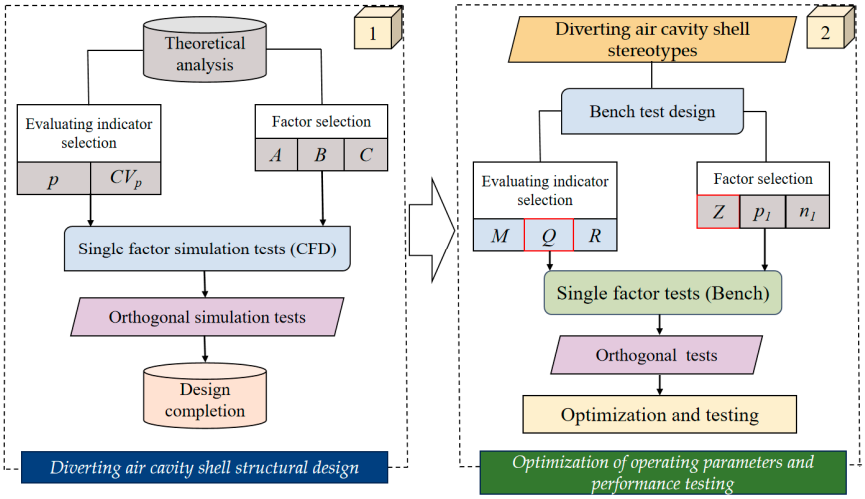

Figure 1. Material and method flow chart. The letters in red boxes represent the test factors in the single-factor bench test.

2.1. Structure and Operating Principle

2.1.1. Overall Structure

The structure of the branched air-chamber type pneumatic rice seed metering device is illustrated in Figure 2. This apparatus consists of several components, including a seed hopper, seed feed tube, seed metering device casing, seed cleaning brush, seed metering shaft, viewing panel, seed discharge plate, intermediate air chamber casing, branched air chamber casing, adjustable multi-hole seed metering disc, air chamber control board, debris cleaning brush, seed metering tube, and seed collection port.

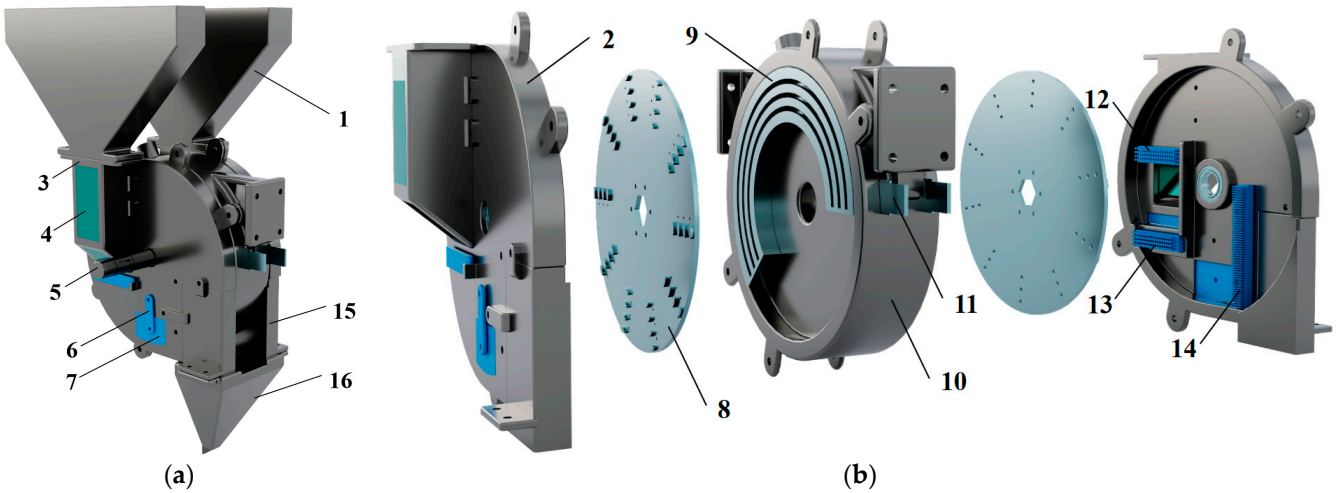

Figure 2. Schematic of the seed metering device. 1. Seed hopper. 2. Seed metering device casing. 3. Seed feed tube. 4. Viewing panel. 5. Seed metering shaft. 6. Connector. 7. Seed discharge plate. 8. Adjustable multi-hole seed metering disc. 9. Branched air chamber casing. 10. Intermediate air chamber casing. 11. Air chamber control board. 12. Seed cleaning brush. 13. Seed separating brush. 14. Debris cleaning brush. 15. Seed metering tube. 16. Seed collection port. (**a**) Side front view. (**b**) Internal structure view.

2.1.2. Operating Principle

The seed metering device is divided into several zones: seed loading, seed cleaning, seed transporting, seed discharging, and transition, as shown in Figure 3. During operation,

rice seeds in the seed hopper move due to gravity through the seed feed tube into the seed loading zone of the metering device. At this point, seeds are adhered to the suction holes on the seed metering disc. Driven by the seed metering shaft, the disc rotates clockwise. When the disc reaches the seed cleaning zone, the seed cleaning brush removes excess seeds, ensuring that only one seed remains at each suction hole. In the seed transporting zone, seeds continue to be held by the suction holes until they reach the seed discharging zone. Once the negative pressure at the suction holes is discontinued, the seeds, under the combined influence of gravity and centrifugal force, pass through the seed metering tube into the seed collection port, where they are aggregated and dispensed, completing the seed metering process. Subsequently, the seed metering disc enters the transition zone, where the debris cleaning brush removes any impurities from the suction holes to ensure smooth operation in the next cycle, before the disc re-enters the seed loading zone to begin another round.

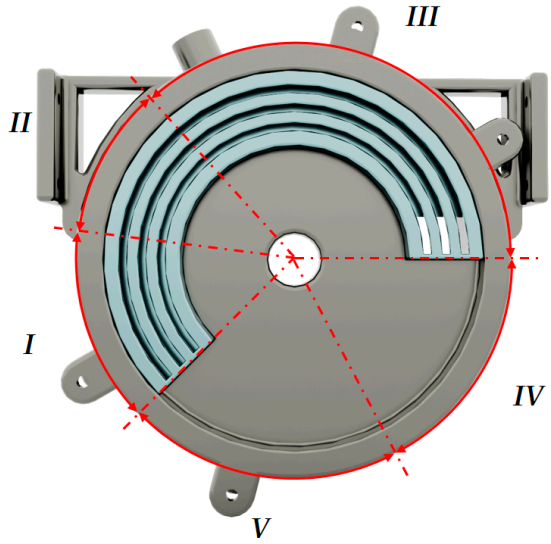

Figure 3. Operational zones of the seed metering device. *I*. Seed loading zone. *II*. Seed cleaning zone. *III*. Seed transporting zone. *IV*. Seed discharging zone. *V*. Transition zone.

2.1.3. Principle of Seeding Rate Adjustment

As illustrated in Figure 4, during the operation of the seed metering device, negative pressure air enters the common air chamber of the intermediate air chamber casing through the air intake. At this initial state, the air chamber control board is fully inserted, connecting or isolating the common air chamber from the independent air chambers through ventilation slots located at the bottom of the branched air chamber casing. By adjusting the insertion depth of the air chamber control board into the ventilation slots, connectivity between the common air chamber and the independent air chambers can be either established or blocked. Initially, all independent air chambers are isolated by the air chamber control board, maintaining negative pressure only in the common air chamber. When the air chamber control board is withdrawn to a certain depth, the common air chamber connects to an independent air chamber, thereby causing rice seeds to adhere to the suction holes on the seed metering disc under the negative pressure in that chamber. Since the other independent air chambers remain isolated, only one suction hole attracts rice seeds. By adjusting the position of the air chamber control board, the connectivity between the six independent air chambers on the left and right branched air chamber casings and the common air chamber can be controlled, allowing for the adjustment of 1 to 6 suction holes, and thus altering the seeding rate.

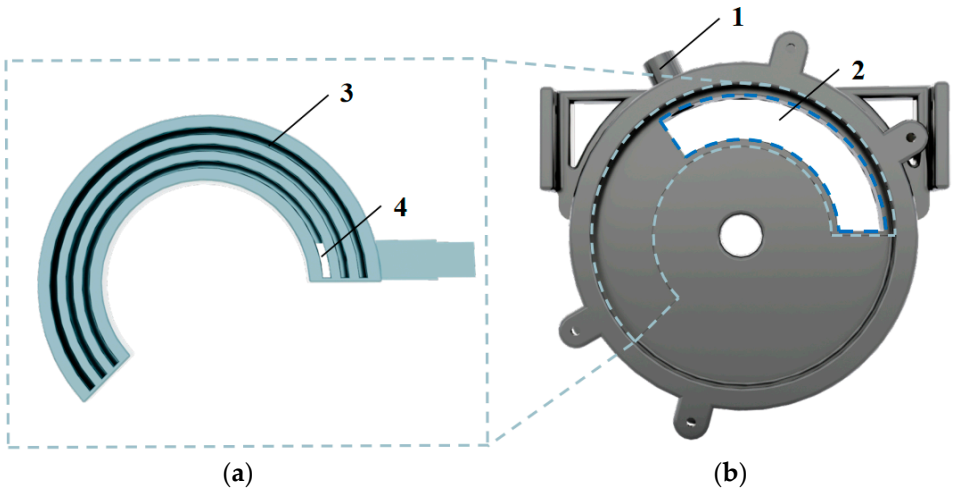

Figure 4. Schematic of the main components for seeding rate adjustment. 1. Air intake. 2. Common air chamber. 3. Independent air chambers. 4. Ventilation slots. (**a**) Intermediate air chamber casing. (**b**) Branched air chamber casing.

2.2. Key Component Design

2.2.1. Design of the Adjustable Multi-Hole Seed Metering Disc

In paddy field operations, the typical walking speed of agricultural machinery is generally between 0.5 and 1 m/s [26]. During direct seeding of rice, the spacing between seed holes is usually controlled within a range of 0.15 to 0.25 m [27]. According to Equation (1), the number of groups of suction holes on the seed metering disc should be between 10 and 14. If the spacing between suction holes is too small, it can increase interference between rice seeds, thereby affecting the effective separation of the seeds. Therefore, under a constant rotational speed n_d, fewer groups of suction holes Z_0 result in better seed suction performance. Based on this, the number of suction hole groups Z_0 on the seed metering device is set to 10 to ensure optimal seed suction performance.

$$Z_0 = \frac{60 v_b}{s n_d} \tag{1}$$

where:

Z_0—the number of suction hole groups;
v_b—the forward speed of the seed planter, m/s;
s—the seed hole spacing during direct seeding of rice, m.

The magnitude of the suction force of the suction holes directly determines the seed suction performance of the seed metering device. The negative pressure required at the suction hole to adhere rice seeds should satisfy the following:

$$\begin{cases} F_p = Sp \\ Q_v = Sv_e \\ p + \rho g h + \frac{1}{2}\rho v_e^2 = C \\ S = (k_2 - k_1)\frac{2Q_v}{\pi d} \end{cases} \tag{2}$$

where:

F_p—the suction force at the suction hole, N;
S—the surface area affected by airflow on the seed, m^2;
p—the negative pressure at the suction hole, Pa;
Q_v—the airflow rate, m^3/s;
v_e—the airflow speed, m/s;
ρ—the air density, kg/m^3;
h—the vertical height, m;
C, k_1, and k_2—constants.

From Equation (2), we derive

$$F_p = \frac{2Q_v}{\pi d}(C - \rho g h)(k_2 - k_1) - \frac{Q_v \rho \pi d}{4(k_2 - k_1)} \quad (3)$$

Equation (3) indicates that the suction force F_p at the suction hole is directly proportional to the airflow rate Q_v and inversely proportional to the diameter of the suction hole. Reducing the diameter d can increase the suction force F_p, but d must be greater than the minimum diameter of the rice seeds. The commonly used rice varieties selected for this study include Super Hybrid Rice Y-2 You 900, Common Hybrid Rice Pei Za Tai Feng, and Conventional Rice Huang Hua Zhan, with widths of 2.31 mm, 2.34 mm, and 2.26 mm, respectively. According to the "Agricultural Machinery Design Manual" [28], the diameter d of the suction hole should be between 1.44 and 1.54 mm (see Equation (4)), thus the suction hole diameter is set at 1.44 mm.

$$d = (0.64 \sim 0.66)b \quad (4)$$

where:

b—the average width of the rice seeds, m.

2.2.2. Design of the Branched Air Chamber Casing

The branched air chamber casing contains three rows of independent and symmetrical air chambers, with a total arc length of 220 degrees. The seed metering device utilizes the negative pressure provided by the branched air chamber casing to create a pressure differential between the seed metering disc and the external environment. This differential enables the adhesion of rice seeds to the suction holes on the seed metering disc, thereby facilitating the seed suction process. As such, the magnitude and stability of the negative pressure at the suction holes are critical factors affecting the seed suction performance of the seed metering device.

To further determine the minimum critical negative pressure required for stable adhesion of rice seeds by the metering device, the following theoretical analysis was conducted: During the seed suction process, the forces acting on the rice seeds primarily include the adhesive force F_p from the suction holes, the seeds' own gravitational force G, the frictional force F_f between the seeds and the seed metering disc, and the inertial force F_i generated by the rotation of the seed metering disc. Given the three-row structure of suction holes on the disc, the outermost row experiences the greatest inertial force F_i. To ensure reliable adhesion of rice seeds by each row of suction holes during operation, this analysis focuses on the outermost row of suction holes, as illustrated in Figure 5.

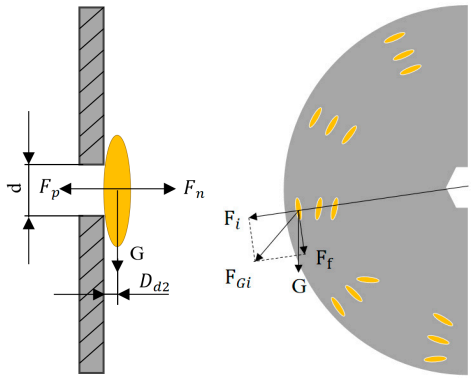

Figure 5. Force diagram of seed suction. F_n represents the supportive force from the seed metering disc on the rice seeds, N; F_p is the adhesive force from the suction holes on the rice seeds, N; D_{d2} is the distance between the center of gravity of the rice seed and the seed metering disc, m; F_i signifies the inertial force from the seed metering disc on the rice seeds, N; F_f is the frictional force between the seed metering disc and the rice seeds, N; F_{Gi} is the resultant force of G and F_i, N.

From Figure 5, it is observed that the gravitational force G, the frictional force F_f, and the inertial force F_i generated by the rotation of the seed metering disc can be expressed as a combined force F_c using the vector sum method as shown in Equation (5):

$$\begin{cases} F_i = \frac{2\pi}{60} D_{d1} m n_d \\ \vec{F_c} = \vec{G} + \vec{F_i} + \vec{F_f} \end{cases} \tag{5}$$

where:

F_c—the combined force acting on the rice seeds, N.

From Equation (5), we derive

$$\begin{cases} F_{G_i} = \left(G^2 + F_i^2 + 2GF_i\cos\gamma\right)^{\frac{1}{2}} \\ F_c = \left({F_{G_i}}^2 + F_f^2 + 2F_{G_i}F_f\cos\varepsilon\right)^{\frac{1}{2}} \end{cases} \tag{6}$$

where:

γ—the angle between G and F_i, (°);

ε—the angle between F_c and F_{Gi}, (°).

From Equation (6), the torque balance condition for a single suction hole adhering rice seeds can be stated as follows:

$$p = \frac{2D_{d2}}{d}\left({F_{G_i}}^2 + F_f^2 + 2F_{G_i}F_f\cos\varepsilon\right)^{\frac{1}{2}} \tag{7}$$

In field conditions, the seed metering device is also subject to external environmental factors such as vibrations and impacts. Therefore, it is necessary to incorporate an environmental reliability coefficient O_1 and an adhesion reliability coefficient O_2 [29], leading to

$$p = \frac{2D_{d2}O_1O_2}{d}\left({F_{G_i}}^2 + F_f^2 + 2F_{G_i}F_f\cos\varepsilon\right)^{\frac{1}{2}} \tag{8}$$

where:

O_1—the environmental reliability coefficient;

O_2—the adhesion reliability coefficient.

Considering that the seed metering device must maintain stable seed suction under all extreme angular conditions, setting $cos\gamma = cos\varepsilon = 1$ yields the maximum critical negative pressure at the suction holes as follows:

$$p = \frac{2D_{d2}O_1O_2}{d}\left(1 + \frac{v^2}{D_{d1}g} + \lambda\right) \tag{9}$$

where:

λ—the comprehensive coefficient of frictional resistance for the rice seeds.

From Equation (9), it is apparent that the negative pressure at the suction holes is closely related to various factors including the position of the rice seed's center of gravity, the linear speed of the suction holes v_d, the diameter of the suction holes d, and the operating environment. During operation, the negative pressure at the suction holes should exceed the theoretically calculated critical minimum negative pressure to effectively reduce the rate of missed seeds and enhance the performance of the seed metering device. Preliminary tests, as referenced in [30], indicate that when the negative pressure in the seed metering device's air chamber is increased to 1300 Pa, the suction holes can stably adhere rice seeds. According to the suction hole structural parameters designed in Section 2.2.1, the diameter of the suction holes on the seed metering disc is 1.44 mm; therefore, the negative pressure at the suction holes should not be less than 800 Pa.

In engineering, the structural parameters of critical components in airflow fields determine the airflow volume and its stability through the conduits [31]. The branched air

chamber casing is a core component of the fluid domain for the seed metering device, with major structural parameters including the depth of the air chamber, the angular extent of the air chamber, and the depth of the air cavity. To explore the effects of these three factors on the magnitude and stability of the negative pressure at the suction holes of the seed metering disc, and thereby determine optimal structural parameters, this study conducted simulation tests using the fluid simulation software Ansys-Fluent (2021 R1).

2.3. Simulation Test Methods

2.3.1. Evaluation Metrics

From the theoretical analysis in Section 2.2.1, it is known that the factors affecting the seed suction performance of the seed metering device are the magnitude and stability of the negative pressure at the suction holes. Under identical inlet negative pressure conditions, higher negative pressures and lower coefficients of variation in these pressures indicate better performance of the branched air chamber casing. Consequently, the negative pressure at the suction holes (p) and the coefficient of variation of this pressure (CV_p) were determined as the evaluation metrics for the simulation tests. The equation for calculating CV_p is as follows:

$$CV_p = \left(\frac{\sigma}{\mu}\right) \times 100\% \tag{10}$$

where:

σ—the standard deviation of p, and μ is the mean value of p.

2.3.2. Simulation Test Setup

The seed metering disc is designed with 10 groups of suction holes, encompassing an overall arc length of 220°, allowing for a maximum of six groups of suction holes to be positioned simultaneously over the negative pressure air cavity. The geometric modeling was conducted using SolidWorks (2020) software, and the model was saved in STEP format and imported into the Workbench Geometry for fluid domain division (as shown in Figure 6a). Subsequently, the inlet and outlet were defined, and the model was imported into Workbench Meshing (2021 R1) software for fluid domain mesh division (as shown in Figure 6b).

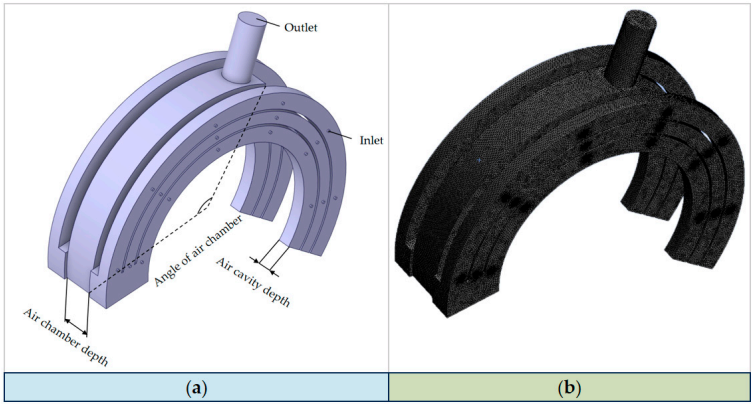

Figure 6. Fluid domain model and mesh division schematic. (**a**) Fluid domain geometric model. (**b**) Fluid domain mesh.

The mesh file was then imported into the Ansys-Fluent fluid simulation software. Within Fluent, boundary conditions were set with the seed metering device's pressure inlet at 0 kPa and the pressure outlet at −1300 Pa. The standard k-ε turbulence model was selected as the viscosity model, and the solution scheme utilized the SIMPLE algorithm. Momentum was modeled using a first-order upwind differencing scheme, and the model walls were set as no-slip. Lastly, the upper and lower limits of negative pressure were

defined, the maximum number of iterations was set to 2000, and the convergence criterion was set at 0.0001. After performing a hybrid initialization, the computation commenced.

Upon completion of the calculations, post-processing of the simulation results was carried out, and the negative pressure values for 36 suction holes across six groups were exported to calculate their average and the coefficient of variation, CV_p.

2.3.3. Single-Factor Simulation Test Method

In order to determine the optimal structural parameters of the branched air chamber casing, p and CV_p were chosen as evaluation criteria. The test factors included air chamber depth, chamber angle, and air cavity depth. Following the methods described in the referenced literature [31], a single-factor simulation test was conducted. In this approach, each test group altered only one factor while keeping the others constant. Each set of trials was repeated three times, and the mean values were calculated. The arrangement of these tests is outlined in Table 1.

Table 1. Single-Factor Test Factors and Levels.

Level	Air Chamber Depth/mm	Air Chamber Angle/(°)	Air Cavity Depth/mm
1	14, 16, 18, 20, 22	100	25
2	22	90, 100, 110, 120, 130	25
3	22	100	15, 17.5, 20, 22.5, 25

2.3.4. Orthogonal Simulation Test Method

To clarify the impacts of the air chamber depth, angular extent, and air cavity depth on $L_9(3^4)$ and CV_p, an orthogonal test based on the results of the single-factor test was conducted using an $L_9(3^4)$ orthogonal array for these three factors. Factors A, B, and C represent the levels of these parameters, as shown in Table 2. The test arrangements are detailed in Table 3.

Table 2. Orthogonal Simulation Test Factors and Levels.

Level	Air Chamber Depth A/mm	Air Chamber Angle B/(°)	Air Cavity Depth C/mm
1	18	90	20
2	20	100	22.5
3	22	110	25

Table 3. $L_9(3^4)$ Orthogonal Simulation Test Arrangements and Results.

Test No.		Factors			p/Pa	CV_p/%
		A	B	C		
1		1	1	1	691	1.14
2		1	2	2	734	1.02
3		1	3	3	752	1.65
4		2	1	2	742	1.09
5		2	2	3	775	0.95
6		2	3	1	721	1.56
7		3	1	3	852	1.07
8		3	2	1	798	0.90
9		3	3	2	825	1.43
p	k_1	726	762	737		
	k_2	746	769	767		
	k_3	825	766	793		
	R	99	7	56		
Primary and Secondary Order		A > C > B				
Optimized combination		$A_3B_2C_3$				

Table 3. *Cont.*

Test No.		Factors			*p*/Pa	CV_p/%
		A	B	C		
CV	k_1	1.27	1.10	1.20		
	k_2	1.20	0.96	1.18		
	k_3	1.13	1.54	1.22		
	R	0.14	0.58	0.04		
Primary and Secondary Order		B > A > C				
Optimized combination		$A_3B_2C_2$				

2.3.5. Verification Test Method

To verify the accuracy of the optimization results, simulation verification test was performed under the same conditions, repeated three times to obtain an average. To further explore the pressure magnitudes in the negative pressure flow field at the suction holes under these conditions, the suction holes were numbered in six groups as shown in Figure 7, and cross-sectional planes through the center of the holes were sliced and numbered accordingly.

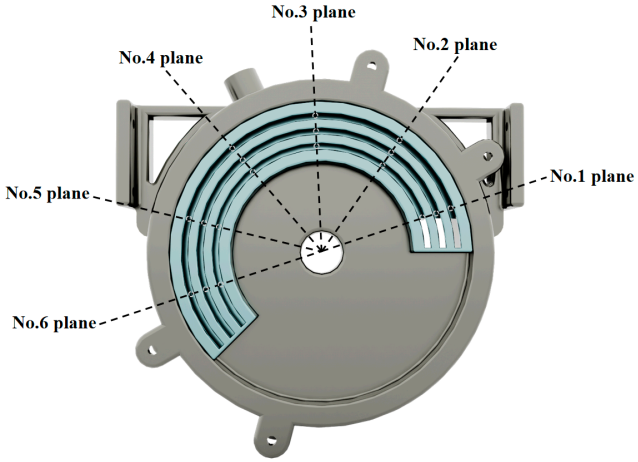

Figure 7. Schematic diagram of the suction hole slice plane division. No.1 plane. For the first suction hole No.2 plane. For the second suction hole No.3 plane. For the third suction hole No.4 plane. For the fourth suction hole No.5 plane. For the fifth suction hole No.6 plane. For the sixth suction hole.

2.4. Bench Test Method

2.4.1. Test Bench Setup

To determine the optimal operating parameters of the seed metering device under varying seeding rate requirements, test materials were selected for seeding targets of 13 seeds per hole, 24 seeds per hole, and 5–8 seeds per hole. These included super hybrid rice, normal hybrid rice, and conventional rice. Drawing from the optimization results of simulations performed with Ansys-Fluent, the bench test setup used a branched air chamber casing with a chamber depth of 22 mm, chamber angle of 100°, and air cavity depth of 25 mm. The tests were conducted on 28 June 2024, at the Intelligent Agricultural Machinery Equipment Engineering Laboratory of Hainan University using the PTS1-03 test bench as illustrated in Figure 8.

The super hybrid rice variety used in the bench tests was Y-2 You 900, with a moisture content of 23.18% and average triaxial dimensions (length × width × thickness) of 8.93 mm × 2.31 mm × 1.79 mm; the normal hybrid rice variety was Pei Za Tai Feng, with a moisture content of 22.87% and average dimensions of 8.97 mm × 2.34 mm × 1.86 mm; the conventional rice variety was Huang Hua Zhan, with a moisture content of 22.35% and average dimensions of 9.52 mm × 2.26 mm × 1.97 mm.

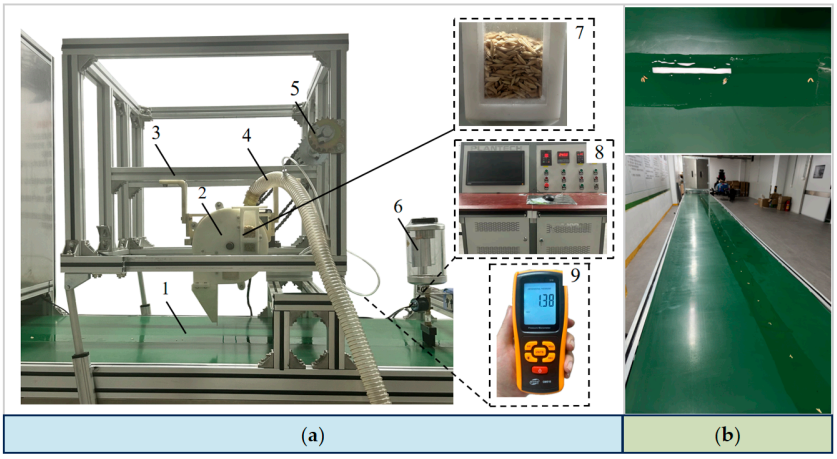

Figure 8. Test bench. 1. Drive belt. 2. Seed metering device. 3. Bench. 4. Air hose. 5. Drive system. 6. Oil supply device. 7. Test seeds. 8. Control system. 9. Pressure gauge. (**a**) Seeding test bench. (**b**) Planting effect drawing.

2.4.2. Evaluation Criteria

In accordance with the Chinese National Standard GB/T6973-2005 for single-grain precision seed metering device testing, and aligned with the agronomic requirements for direct seeding of rice, the evaluation criteria selected were the miss rate M, qualification rate Q, and reseeding rate R. The calculation methods for each criterion are as follows:

$$\begin{cases} M_{s,h,r} = \frac{n_{M_s,M_h,M_r}}{N} \times 100\% \\ Q_{s,h,r} = \frac{n_{Q_s,Q_h,Q_r}}{N} \times 100\% \\ R_{s,h,r} = \frac{n_{R_s,R_h,R_r}}{N} \times 100\% \end{cases} \tag{11}$$

where:

M—the miss rate (%);
Q—the qualification rate (%);
R—the reseeding rate (%);
N—the total number of holes counted per trial group;
s—super hybrid rice;
h—normal hybrid rice;
r—conventional rice.

For super hybrid rice, n_{Ms} indicates the total number of missed holes, n_{Qs} counts the holes with 13 seeds meeting the standard, and n_{Rs} identifies holes needing reseeding with more than 3 seeds. For normal hybrid rice, n_{Mh} counts the holes with fewer than 2 seeds missed, n_{Qh} counts the holes with 24 seeds meeting the standard, and n_{Rh} identifies holes needing reseeding with more than 4 seeds. For conventional rice, n_{Mr} counts the holes with fewer than 5 seeds missed, n_{Qr} counts the holes with 5–8 seeds meeting the standard, and n_{Rr} identifies holes needing reseeding with more than 8 seeds.

During the tests, the seed output of each hole by the seed metering device was continuously recorded. Every 250 holes constituted a trial group, with each group being repeated three times to calculate the average values.

2.4.3. Single-Factor Bench Test

In accordance with the principles of adjustable seeding rates outlined in Section 2.1.3, the seed metering device can control the connection or disconnection of 1 to 6 suction holes, thus adjusting the seeding rate. To investigate the optimal number of open holes (Z) for various seeding rate requirements, as well as to determine appropriate values for working vacuum pressure (p_1) and rotational speed (n_1), single-factor bench tests were conducted.

(1) Test on Number of Open Holes

To ascertain the optimal number of open holes (Z) for different seeding rates, the qualification rate was used as the evaluation criterion. Z was set at six levels: 1, 2, 3, 4, 5, and 6. The working vacuum pressure was fixed at 1300 Pa, and the rotational speed was maintained at 30 r/min. A single-factor bench test was carried out under these conditions.

(2) Single Factor Test of Negative Pressure in Work

Identifying the suitable working vacuum pressure (p_1) is crucial for enhancing the performance of the pneumatic seed metering device. The qualification rate served as the evaluation criterion. The test levels were set at 700, 1000, 1300, 1600, and 1900 Pa. For seeding targets of 1–3 seeds, 2–4 seeds, and 5–8 seeds per hole, Z was set to 2, 3, and 6 holes, respectively, with a constant rotational speed (n_1) of 30 r/min. Single-factor bench tests were conducted for each setting.

(3) Test on Working Vacuum Pressure

To explore the impact of rotational speed (n_1) on the operational performance of the seed metering device, qualification rate was again used as the evaluation criterion. The levels tested were 10, 20, 30, 40, and 50 r/min, with the working vacuum pressure fixed at 1300 Pa. The conditions were otherwise identical to those in the vacuum pressure single-factor test.

2.4.4. Regression-Orthogonal Design Methodology

(1) Test Method

To determine the optimal combination of operating parameters for the seed metering device, the test was guided by indicators such as miss-seeding rate, qualification rate, and re-seeding rate. Based on the conclusions from the single-factor bench tests, the range for working vacuum pressure was set between 1000 to 1600 Pa, and rotational speed was set between 20 to 40 r/min. For seeding targets of 1–3 seeds, 2–4 seeds, and 5–8 seeds per hole, the number of open holes was set at 2, 3, and 6, respectively, and an orthogonal test was conducted. The test utilized a four-level check ($m_0 = 4$) with $r = 1.21$, and results were analyzed using Design-Expert 12 software. The design of test factor levels is shown in Table 4, the encoding method for test factors is shown in Table 5, and the test arrangements is outlined in Table 6.

Table 4. Regression-Orthogonal Test Factors and Levels.

Level	Working Pressure X_1/Pa	Working Speed X_2/(r/min^{-1})
1	1000	20
2	1300	30
3	1600	40

Table 5. Regression-Orthogonal Test Factor Encoding.

Code	Working Pressure X_1/Pa	Working Speed X_2/(r/min^{-1})
$r(X_{2j})$	1600	40
$1(X_{0j} + \Delta_j)$	1547.93	38.26
$0(X_{0j})$	1300	30
$1(X_{0j} - \Delta_j)$	1052.06	21.73
$-r(X_{1j})$	1000	20
$\Delta_j = (X_{2j} - X_{1j})/2r$	247.93	8.26
$x_j = (X_j - X_{0j})/\Delta_j$	$x_1 = 0.004(X_1 - 1300)$	$x_2 = 0.121(X_2 - 30)$

Note: Δ_j is the j-th factor's minimal change interval, $j = 1, 2$; the encoded factors is x_j and the asterisk arm is r.

Table 6. Regression-Orthogonal Test Arrangements.

Test	X_0	X_1	X_2	X_1 X_2	$X_1{}^2$	$X_2{}^2$
1	1	1	1	1	1	1
2	1	1	−1	−1	1	1
3	1	−1	1	−1	1	1
4	1	−1	−1	1	1	1
5	1	r	0	0	r^2	0
6	1	$-r$	0	0	r^2	0
7	1	0	r	0	0	r^2
8	1	0	$-r$	0	0	r^2
9	1	0	0	0	0	0
10	1	0	0	0	0	0
11	1	0	0	0	0	0
12	1	0	0	0	0	0

Note: X_j is the encoded factor, with j = 1 or 2, and r being the asterisk arm.

(2) Regression Method

Following the orthogonal analysis and variance analysis, insignificant terms and interactions were removed for a multivariate fitting. This process derived regression equations for the miss-seeding rate (M), qualification rate (Q), and re-seeding rate (R) under the seeding targets for each seed quantity category.

(3) Multi-Objective Optimization Method

To obtain the best operational parameters for the seed metering device, a multi-objective optimization was performed, taking into account the real-world operating conditions of the device and the impact of these parameters on testing indicators. The optimization was formulated as follows:

$$\begin{cases} \min M \\ \max Q \\ \min R \\ 1000\ \text{Pa} \le X_1 \le 1600\ \text{Pa} \\ 20\ \text{r/min} \le X_2 \le 40\ \text{r/min} \end{cases} \tag{12}$$

(4) Validation Test Method

A bench validation test was conducted based on the multi-objective optimization results.

3. Results

3.1. Simulation Test Results

3.1.1. Single-Factor Simulation Test Results

The results of the single-factor simulations are presented in Figures 9–11.

Figure 9 illustrates the effect of chamber depth on p and CV_p. The results indicate a significant increasing trend in pressure as chamber depth increases, peaking at 22 mm. Concurrently, CV_p gradually decreases, especially within the range of 18 mm to 22 mm, showing increased stability and consistency. Given the spatial constraints of the seed metering device assembly process, the feasible range for chamber depth was set between 18 mm and 22 mm.

Figure 10 displays how chamber angle influences p and CV_p. As the chamber angle increases, p shows a gradual upward trend, reaching a maximum at 130°. Notably, CV_p exhibits a nonlinear trend of decreasing and then increasing with changes in chamber angle, indicating optimal uniformity and stability of suction hole pressure within the range of 90° to 110°. Based on test data and process analysis, the chamber angle was set within this range to optimize the performance of the seed metering device.

Figure 11 elucidates the relationship between cavity depth and its effects on p and CV_p. The results show that with an increase in cavity depth, p continuously rises, reaching its highest at 25 mm; simultaneously, CV_p continuously decreases, indicating that the distribution of suction hole pressure achieves optimal stability and uniformity within the range of 20 mm to 25 mm. Considering structural assembly and spatial constraints of the seed metering device, the optimal range for cavity depth was determined to be 20 mm to 25 mm.

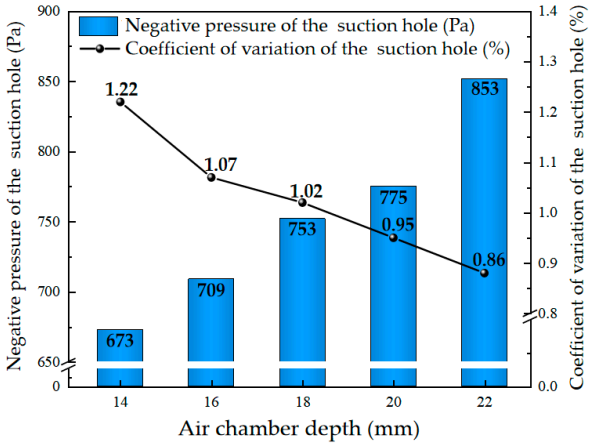

Figure 9. Impact of chamber depth on performance in single-factor tests.

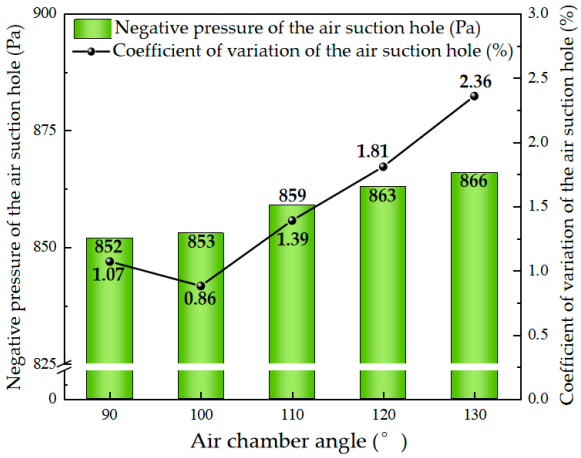

Figure 10. Impact of chamber angle on performance in single-factor tests.

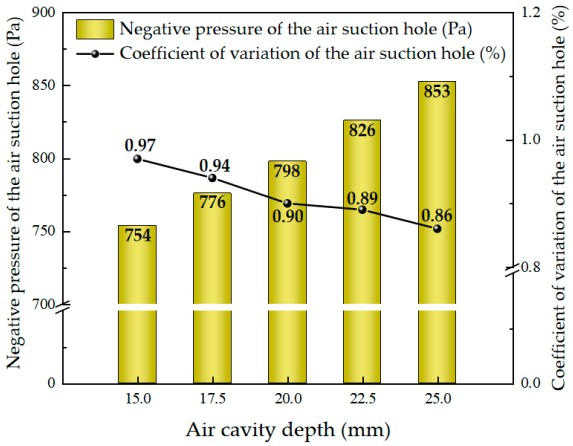

Figure 11. Impact of cavity depth on performance in single-factor tests.

3.1.2. Orthogonal Simulation Test Results

The results of the orthogonal test are presented in Table 3, and the analysis of variance (ANOVA) results are shown in Table 7.

Table 7. ANOVA of Orthogonal Simulation Test.

Metrics	Source	*SS*	*df*	*MS*	*F*-Value	Significance
p	A	16,521.56	2	8260.78	308.49	**
	B	81.56	2	40.78	1.52	
	C	4769.56	2	2384.75	89.06	*
	e	53.56	2	26.78		
	Sum	21,426.24	8	10,713.09		
CV_p	A	0.0280	2	0.014	8.00	*
	B	0.5682	2	0.2841	180.38	**
	C, e (e^{Δ})	0.0028, 0.0035 (0.0063)	2, 2 (4)	0.001575		
	Sum	0.6025	8	0.299675		

Note: Critical value of *F*-test: $F_{0.05}$ (2,2) = 19.00, $F_{0.01}$ (2,2) = 99.00; $F_{0.05}$ (2,4) = 6.94, $F_{0.01}$ (2,4) = 18.00. "*" means the factor is significant when α = 0.05, "**" means the factor is significant when α = 0.01.

The orthogonal test and ANOVA results indicate the order of influence of factors on p from greatest to least is A (chamber depth), C (cavity depth), and B (chamber angle), with chamber depth having a highly significant impact on p and a significant impact on CV_p. Chamber angle shows a highly significant influence on CV_p, whereas the impact of cavity depth on CV_p is not significant. The optimal combinations were identified as A_3,B_2,C_3, and A_3,B_2,C_2. Given the negligible differences between C_2 and C_3, the optimal parameter combination was finalized as A_3, B_2 and C_3, corresponding to a chamber depth of 22 mm, chamber angle of 100°, and cavity depth of 25 mm.

3.1.3. Verification Test Results

The results of the validation tests are presented in Figure 11, derived from the post-processing data using Ansys-Fluent. The average negative pressure was recorded at 857 Pa with a coefficient of variation of 0.86%. As clearly illustrated in Figure 12, the pressure p significantly exceeds the minimum critical negative pressure of 800 Pa, which was theoretically calculated in Section 2.2.2. Consequently, the pressures at all suction holes are sufficient to ensure stable adhesion of the rice seeds.

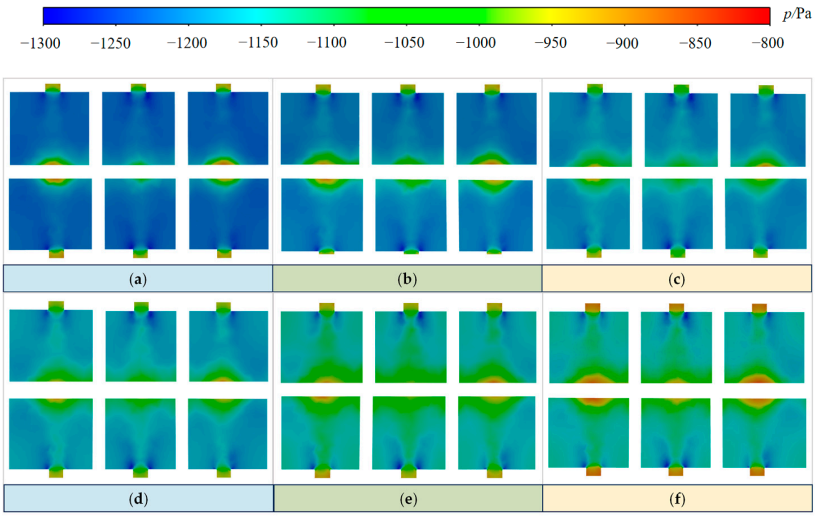

Figure 12. Negative pressure cloud maps of suction holes on slice planes. (**a**) Negative pressure cloud map of the first suction hole slice plane. (**b**) Negative pressure cloud map of the second suction

hole slice plane. (**c**) Negative pressure cloud map of the third suction hole slice plane. (**d**) Negative pressure cloud map of the fourth suction hole slice plane. (**e**) Negative pressure cloud map of the fifth suction hole slice plane. (**f**) Negative pressure cloud map of the sixth suction hole slice plane.

3.2. Bench Test Results

3.2.1. Single Factor Bench Test Results

The results of the single-factor tests are depicted in Figures 13–15.

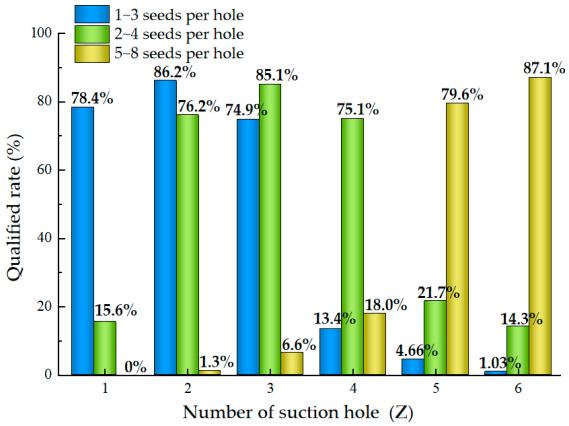

Figure 13. Results of single-factor tests at different numbers of openings.

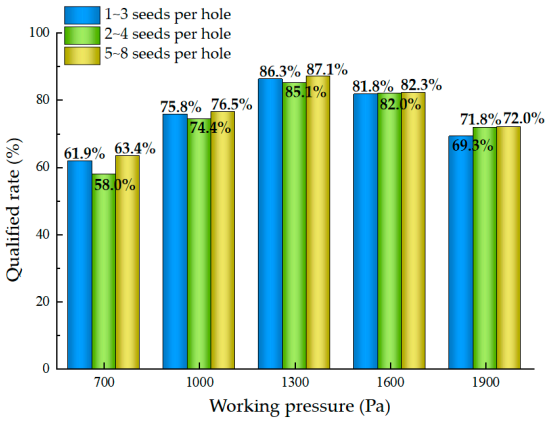

Figure 14. Results of single-factor tests at different working pressures.

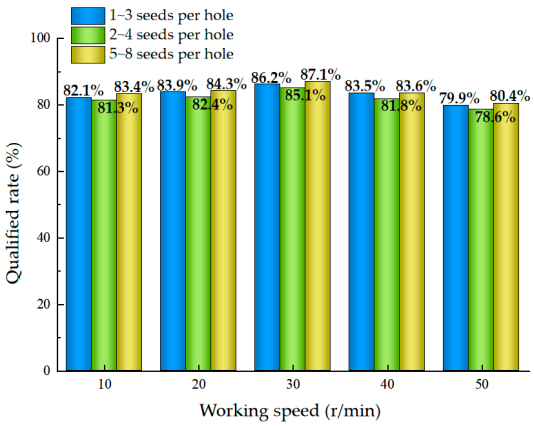

Figure 15. Results of single-factor tests at different rotational speeds.

Figure 13 indicates that the optimal number of openings in the seed metering device is two for targeting 1–3 seeds per hole; three for 2–4 seeds per hole; and six for 5–8 seeds per hole.

As shown in Figure 14, when the pressure p_1 is below 1000 Pa, the qualification rates for all three test groups are significantly below the average. When p_1 exceeds 1600 Pa, the qualification rates markedly decrease. Therefore, the reasonable range for p_1 is determined to be between 1000 and 1600 Pa.

According to the results shown in Figure 15, when the rotational speed n_1 is between 10 and 40 r/min, the qualification rates under varying seeding requirements show minimal changes. A noticeable drop in the qualification rate occurs at 50 r/min. Based on the efficiency requirements for field operations, with walking speeds for paddy field machinery typically ranging from 0.5 to 1 m/s, the rotational speed of the seed metering device should not be less than 20 r/min. Hence, the appropriate range for n_1 was set between 20 and 40 r/min.

3.2.2. Regression-Orthogonal Test Results

(1) Test Results

The results of the regression-orthogonal tests are summarized in Table 8, with the corresponding analysis of variance presented in Table 9.

Table 8. Results of the Regression-Orthogonal Test.

No.	1–3 Seeds per Hole			2–4 Seeds per Hole			5–8 Seeds per Hole		
	M	***Q***	***R***	***M***	***Q***	***R***	***M***	***Q***	***R***
1	9.01	83.83	7.16	8.71	83.77	7.52	8.84	83.20	7.96
2	7.42	79.98	12.60	7.25	81.93	10.82	7.73	80.78	11.49
3	20.14	76.44	3.42	19.76	77.04	3.2	20.81	76.28	2.91
4	27.01	72.54	0.45	26.81	72.85	0.34	26.45	73.34	0.21
5	7.59	82.07	10.34	8.38	82.39	9.23	7.82	82.84	9.34
6	23.35	75.97	0.68	24.12	75.31	0.57	23.33	76.31	0.36
7	3.75	87.28	8.97	4.31	87.64	8.05	4.67	87.48	7.85
8	3.99	87.51	8.50	4.68	85.83	9.49	4.78	88.13	7.09
9	3.59	87.02	9.39	4.19	86.45	9.36	4.38	87.41	8.21
10	4.14	85.95	9.91	3.82	85.53	9.65	4.64	87.61	7.75
11	3.48	86.00	10.52	3.88	85.61	10.51	4.13	87.19	8.68
12	4.35	87.51	10.14	3.65	85.28	11.07	3.71	87.09	9.20

Table 9. Analysis of Variance of Regression-Orthogonal Test.

Source			Model	X_1	X_2	X_1X_2	X_1^2	X_2^2	Residuals	Lack of Fit	Pure Error	Cor Total
1–3 seeds per hole	***M***	***SS***	805.61	357.81	17.89	6.97	201.38	33.59	2.87	2.31	0.56	808.47
		df	5	1	1	1	1	1	6	1	5	11
		MS	161.12	357.81	17.89	6.97	201.38	33.59	0.47	2.31	0.11	
		F	337.22	748.89	37.45	14.59	421.47	70.30		20.53		
		signif	**	**	**	*	**	**		**		
	Q	***SS***	282.66	71.21	0.0006	15.02	84.94	20.58	5.80	2.38	3.42	288.46
		df	5	1	1	1	1	1	6	1	5	11
		MS	56.53	71.21	0.0006	15.02	84.94	20.58	0.96	2.38	0.68	
		F	58.47	73.65	0.0006	15.53	87.85	21.29		3.48		
		signif	**	**		*	**	**				
	R	***SS***	172.44	109.78	17.68	1.53	24.75	1.58	2.28	0.0006	2.88	175.32
		df	5	1	1	1	1	1	6	1	5	11
		MS	34.49	109.78	17.68	1.53	24.75	1.58	0.48	0.0006	0.57	
		F	71.83	228.64	36.83	3.18	51.54	3.30		0.0011		
		signif	**	**	**		**					

Table 9. *Cont.*

Source			Model	X_1	X_2	X_1X_2	X_1^2	X_2^2	Residuals	Lack of Fit	Pure Error	Cor Total
2–4 seeds per hole	*M*	*SS*	796.50	355.89	18.11	7.81	221.86	20.97	2.95	2.23	0.71	799.45
		df	5	1	1	1	1	1	6	1	5	11
		MS	159.30	355.89	18.11	7.81	221.86	20.97	0.49	2.23	0.14	
		F	324.33	724.58	36.89	15.91	451.70	42.69		15.55		
		signif	**	**	**	*	**	**		*		
	Q	*SS*	257.94	85.77	1.38	9.09	81.55	10.49	5.36	1.78	3.57	263.30
		df	5	1	1	1	1	1	6	1	5	11
		MS	51.59	85.77	1.38	9.09	81.55	10.49	0.89	1.78	0.71	
		F	57.79	96.08	1.55	10.18	91.35	11.75		2.49		
		signif	**	**		*	**	*				
	R	*SS*	160.50	92.23	9.49	0.048	34.39	1.80	5.44	0.0250	5.42	165.94
		df	5	1	1	1	1	1	6	1	5	11
		MS	32.10	92.23	9.49	0.048	34.39	1.80	0.90	0.0250	1.08	
		F	35.39	101.69	10.46	0.053	37.92	1.98		0.0231		
		signif	**	**	*		**					
5–8 seeds per hole	*M*	*SS*	762.73	353.05	11.39	5.13	187.82	30.89	3.52	2.70	0.82	766.25
		df	5	1	1	1	1	1	6	1	5	11
		MS	152.55	353.05	11.39	5.13	187.82	30.89	0.58	2.70	0.16	
		F	259.88	601.45	19.41	8.74	319.98	52.62		14.40		
		signif	**	**	**	*	**	**		**		
	Q	*SS*	307.34	71.53	0.0676	7.18	93.85	27.12	2.02	1.34	0.68	309.37
		df	5	1	1	1	1	1	6	1	5	11
		MS	61.47	71.53	0.0676	7.18	93.85	27.12	0.33	1.34	0.13	
		F	182.16	211.98	0.2003	21.29	278.12	80.38		9.88		
		signif	**	**		**	**	**		*		
	R	*SS*	140.18	106.75	9.70	0.172	16.14	0.122	2.99	0.2337	2.76	143.17
		df	5	1	1	1	1	1	6	1	5	11
		MS	28.04	106.75	9.70	0.172	16.14	0.122	0.49	0.2337	0.55	
		F	56.22	214.08	19.46	0.345	32.36	0.245		0.4237		
		signif	**	**	**		**					

Note: Critical value of *F*-test: $F_{0.05}$ (5,5) = 5.050, $F_{0.01}$ (5,5) = 10.96; $F_{0.05}$ (1,5) = 6.60, $F_{0.01}$ (1,5) = 16.25. "*" means the factor is significant when α = 0.05, "**" means the factor is significant when α = 0.01.

(2) Regression Results

For the seeding target of 1–3 seeds per hole, the regression equations for the miss rate *M*, qualification rate *Q*, and double seeding rate *R* are as follows:

$$M = 3.88 - 7.19X_1 + 2.12X_2 - 1.32X_1X_2 + 7.91X_1^2 + 4.10X_2^2 \quad (13)$$

$$Q = 86.55 + 3.21X_1 + 1.94X_1X_2 - 5.14X_1^2 - 3.21X_2^2 \quad (14)$$

$$R = 9.57 + 3.98X_1 - 2.10X_2 - 2.77X_1^2 \quad (15)$$

For the seeding target of 2–4 seeds per hole, the regression equations for the miss rate *M*, qualification rate *Q*, and double seeding rate *R* are as follows:

$$M = 4.09 - 7.17X_1 + 2.13X_2 - 1.40X_1X_2 + 8.31X_1^2 + 3.24X_2^2 \quad (16)$$

$$Q = 86.22 + 3.52X_1 + 1.51X_1X_2 - 5.04X_1^2 - 2.29X_2^2 \quad (17)$$

$$R = 9.69 + 3.65X_1 - 1.54X_2 - 3.27X_1^2 \quad (18)$$

For the seeding target of 5–8 seeds per hole, the regression equations for the miss rate *M*, qualification rate *Q*, and double seeding rate *R* are as follows:

$$M = 4.38 - 7.14X_1 + 1.69X_2 - 1.13X_1X_2 + 7.64X_1^2 + 3.93X_2^2 \quad (19)$$

$$Q = 87.48 + 3.21X_1 + 1.34X_1X_2 - 5.40X_1^2 - 3.68X_2^2 \quad (20)$$

$$R = 8.13 + 3.93X_1 - 1.56X_2 - 2.24X_1^2 \quad (21)$$

(3) Multi-objective Optimization Results

Under various seeding objectives, the optimal operational parameters and test indicators were as follows: When seeding 1–3 seeds per hole, p_1 was set to 1355 Pa and n_1 at 32.78 r/min, achieving a pass rate of 86.78%, with miss and double seeding rates of 3.74% and 9.48%, respectively; for 2–4 seeds per hole, p_1 was set to 1357 Pa and n_1 at 32.87 r/min, with a pass rate of 86.40%, and miss and double seeding rates of 3.91% and 9.69%, respectively; for 5–8 seeds per hole, p_1 was set to 1339 Pa and n_1 at 31.07 r/min, achieving a pass rate of 87.81%, and miss and double seeding rates of 3.71% and 8.48%, respectively.

(4) Validation Test Results

The validation test results were as follows: For seeding 1–3 seeds per hole, the miss rate was 4.70%, pass rate 85.81%, and double seeding rate 9.49%; for 2–4 seeds per hole, the miss rate was 4.60%, pass rate 85.59%, and double seeding rate 9.81%; for 5–8 seeds per hole, the miss rate was 4.09%, pass rate 87.27%, and double seeding rate 8.64%. All test results meet the precision direct seeding requirements for super hybrid rice, common hybrid rice, and conventional rice using a pneumatic seed metering device, and are consistent with the multi-objective optimization results.

4. Discussion

Based on the correlation analysis, it can be inferred that (1) the depth of the air chamber and the depth of the air cavity have a significant impact on p, while the angle of the air chamber significantly affects CV_p; (2) p_1 significantly influences the miss rate, pass rate, and double seeding rate for the three types of rice under various sowing volumes, whereas n_1 only significantly affects the miss rate and double seeding rate, with the degree of impact varying with the sowing volume. This conclusion aligns with the findings of Xing et al. [32], but with a novel approach in this study where the branched air chamber casing is segmented into suction hole slice planes. Additionally, the method of controlling the flow channel of the air chamber through the control board is also an innovative design, which is simpler and more efficient. An analysis and discussion of the potential causes of the test results are presented below.

4.1. Impact of Seed Metering Device Structural Parameters on p and CV_p

4.1.1. Air Chamber Depth

To study the impact of air chamber depth on p and CV_p, an analysis was conducted on the pressure distribution cloud diagrams of the ventilation slots and suction aperture cross-sections at different air chamber depths (as shown in Figure 16).

The results show that with an increase in air chamber depth, the cross-sectional area of the common air chamber expands, leading to changes in the airflow field distribution and a corresponding increase in the negative pressure value of the suction apertures. Figure 16 illustrates significant differences in the negative pressure at the suction aperture cross-sections at depths of 18 mm, 20 mm, and 22 mm. According to the theory of pipeline resistance loss, the loss of gas pressure is inversely proportional to the cross-sectional area of the pipeline. As the air chamber depth increases, the cross-sectional area of the common air chamber enlarges, resulting in reduced pressure loss as the gas enters. Examination of the negative pressure cloud diagrams of the ventilation slot cross-sections in Figure 17 indicates that the negative pressure gas experiences varying degrees of pressure loss in the common air chamber before entering the independent air chambers, causing different negative pressures as the gas passes through the ventilation slots into each independent air chamber, leading to variations in p.

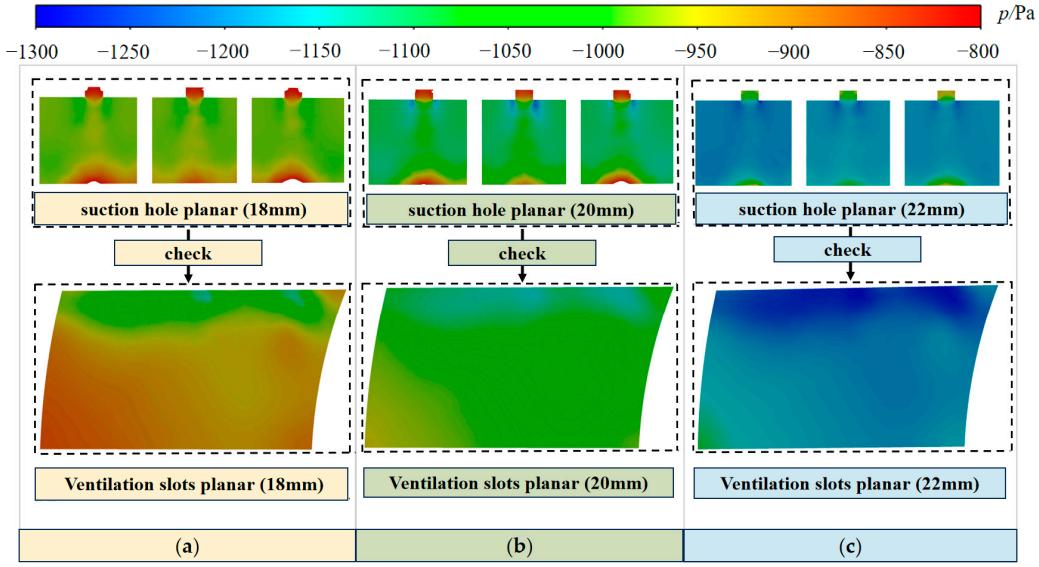

Figure 16. Pressure distribution cloud maps at different air chamber depths for suction holes and ventilation slots. (**a**) 18 mm, (**b**) 20 mm, (**c**) 22 mm.

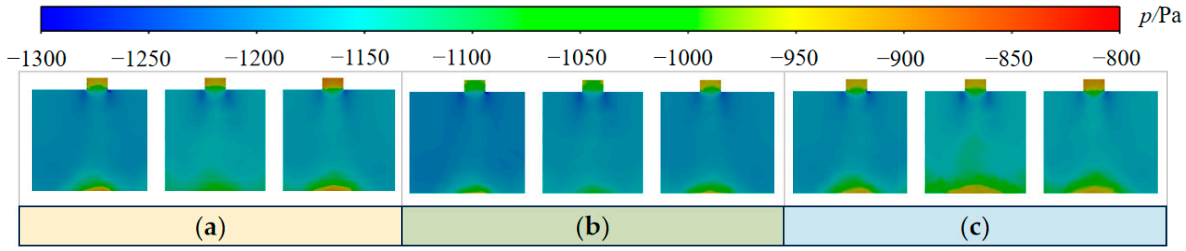

Figure 17. Negative pressure cloud diagrams at different chamber angles. (**a**) 90°, (**b**) 100°, (**c**) 110°.

4.1.2. Air Chamber Angle

The influence of varying chamber angles on p and CV_p was explored by examining pressure cloud diagrams and airflow trajectory maps, as depicted in Figures 17 and 18, respectively. Figure 17 illustrates that when the chamber angle increases from 90° to 100°, the uniformity of the suction aperture's negative pressure improves. This enhancement is attributed to the increased internal space within the chamber, which reduces airflow disturbances and results in more uniform flow, thereby stabilizing the negative pressure and reducing CV_p.

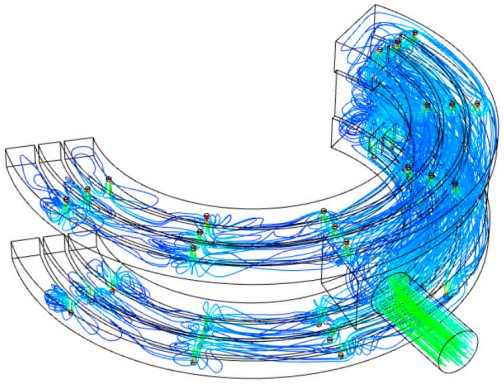

Figure 18. Internal flow lines in the seed metering device.

In contrast, as the chamber angle further increases to 110°, the uniformity of the negative pressure at the suction aperture declines. This decrease is due to structural

constraints, with the position of the ventilation slots fixed at the start of the chamber angle. As shown in Figure 18, the increased distance of the expanded volume from the ventilation slots and the further chamber wall increases the airflow's return path within the common air chamber, reducing the uniformity with which air enters the ventilation slots and consequently decreasing the stability of the negative pressure in both the independent air chamber and the suction apertures. Despite the theoretical expectation that a larger space should enhance negative pressure stability, the longer return distance has a greater detrimental effect on airflow uniformity, thus overall decreasing the stability of negative pressure and increasing CV_p.

4.1.3. Air Cavity Depth

With the increase in cavity depth, p rises, while CV_p remains relatively stable, indicating minor fluctuations. This phenomenon is consistent with the analysis in Section 4.1.1, where the increase in depth of the independent air cavity reduces the pressure loss within the chamber, thus increasing the negative pressure distributed to each suction aperture.

4.2. Impact of Operational Parameters of the Seed Metering Device on Seeding Accuracy

4.2.1. Number of Openings

To investigate the impact of varying the number of openings on the rates of missed seeding, qualification rate, and re-seeding rate, we analyzed the underlying causes based on single-factor bench test results and the statistical data of average seeds sown from 1 to 6 openings. The findings are discussed below.

In tests where 1 to 3 rice seeds per hole were considered acceptable, the qualification rate for the single-opening bench test was 78.42%. Observation through the viewing port of the seed metering device revealed a high incidence of seeds not adhering to the suction apertures, resulting in a high missed seeding rate. The primary reason for this is the barbed and elongated nature of the rice seed surfaces, which increases the difficulty of adhesion within a single suction aperture. In contrast, results from the two-opening test showed a significant increase in qualification rate to 86.26%. This improvement is due to the acceptable seeding range of 1 to 3 seeds per hole, with both missed and re-seeding rates falling within a lower probability range, thereby yielding a higher qualification rate. However, for the three-opening test, the qualification rate dropped to 74.92%, which is notably lower than that for two openings. As depicted in Figure 19, with the increase in the number of openings, the average number of seeds sown reached 2.68, significantly increasing the probability of re-seeding. Additionally, the increase in the number of independent air chambers led to a rise in the coefficient of variation of the internal negative pressure, thus reducing airflow stability and further increasing the likelihood of missed and re-seedings. Consequently, the qualification rate for three openings was lower than that for two openings.

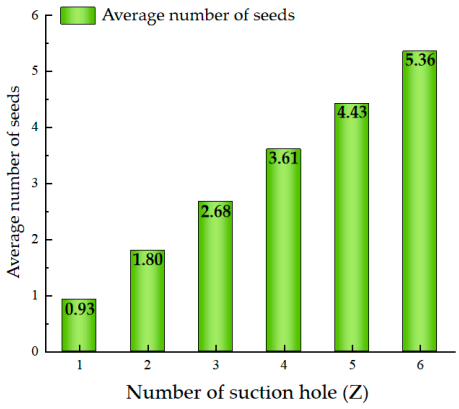

Figure 19. Statistical graph of average number of seeds sown for 1–6 openings.

4.2.2. Working Negative Pressure and Rotor Speed

To elucidate the intrinsic reasons behind the effects of n_1 and p_1 on the missed seeding rate, re-seeding rate, and qualification rate, a response surface analysis was conducted based on bench test results, as shown in Figure 20.

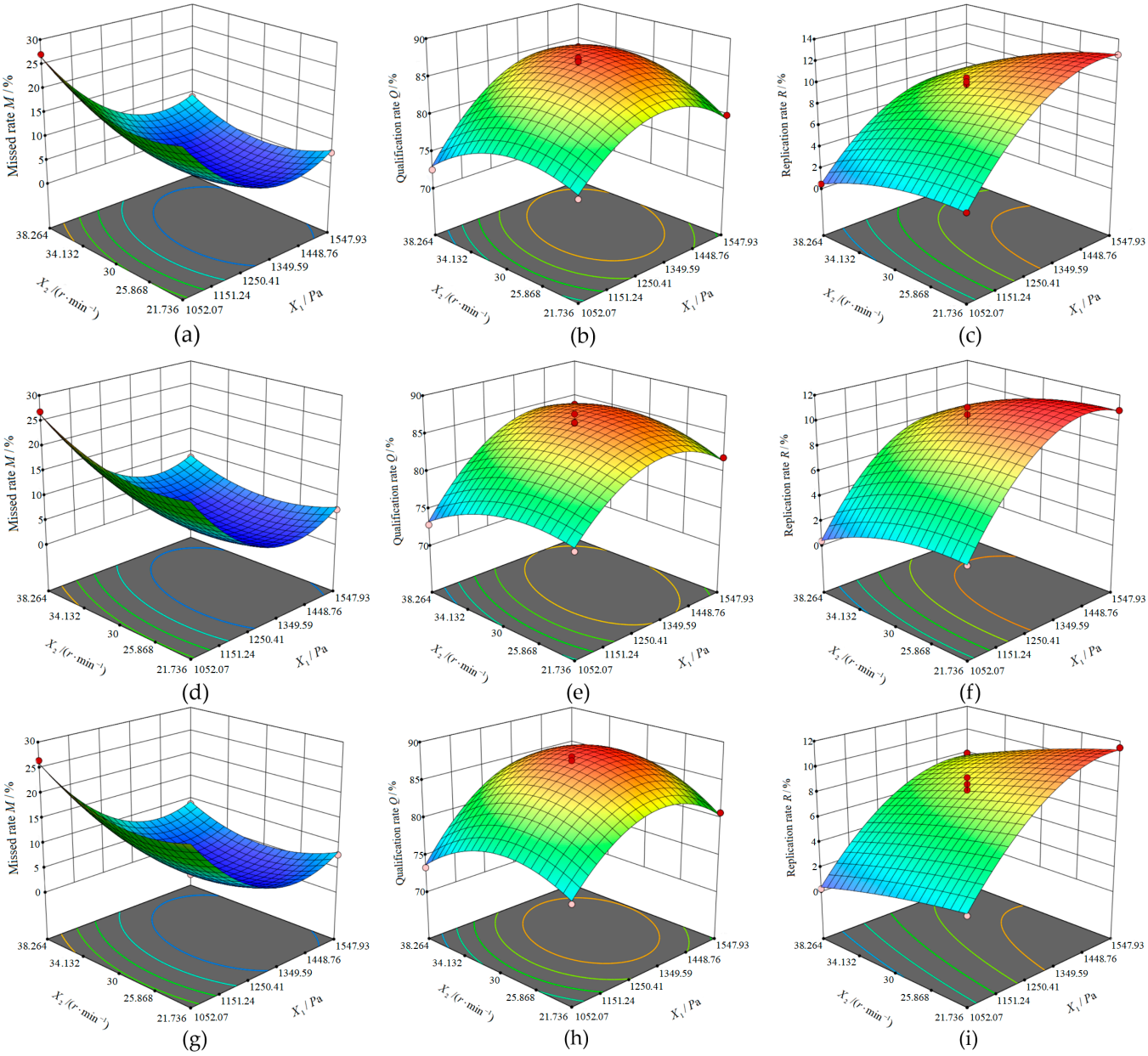

Figure 20. Index of response surfaces of factors. (**a**) The influence on the missed seeding rate for 1–3 seeds. (**b**) The influence on the qualification rate for 1–3 seeds. (**c**) The influence on the re-seeding rate for 1–3 seeds. (**d**) The influence on the missed seeding rate for 2–4 seeds. (**e**) The influence on the qualification rate for 2–4 seeds. (**f**) The influence on the re-seeding rate for 2–4 seeds. (**g**) The influence on the missed seeding rate for 5–8 seeds. (**h**) The influence on the qualification rate for 5–8 seeds. (**i**) The influence on the re-seeding rate for 5–8 seeds.

(1) Impact on Missed Seeding Rate

When n_1 is fixed, the missed seeding rate first significantly decreases and then stabilizes as p_1 increases. According to the theoretical analysis in Section 2.2.2, this phenomenon can be attributed to the suction force at the seed pores, which is directly proportional to the airflow rate and inversely proportional to the pore diameter. Specifically, with a fixed

pore diameter, an increase in working negative pressure raises the airflow rate, thereby enhancing the suction force at the pores, improving the seed pick-up rate, and reducing the missed seeding rate. Once the working negative pressure reaches the threshold necessary for stable seed adhesion to the pores, further increases in pressure do not significantly alter the missed seeding rate.

On the other hand, with p_1 held constant, the missed seeding rate initially decreases and then increases as n_1 rises, reaching its minimum in the range of 25.8–34.1 r/min. At lower rotor speeds, the agitation teeth on the seed metering disc do not significantly disturb the seed population in the loading zone, resulting in poor seed mobility and difficulty in seed suction. As the rotor speed increases, the mobility of the seed population improves, allowing more seeds to be in a state of low interference and thus more easily adhered to, which reduces the missed seeding rate. However, further increases in rotor speed enhance the inertial forces acting on the seeds, reducing the stability of adhesion and leading to "flying seeds", which increase the missed seeding rate. Additionally, higher rotor speeds reduce the residence time of the pores in the loading zone, decreasing the time available for seed adhesion and contributing to an increase in the missed seeding rate.

(2) Impact on Re-seeding Rate

With n_1 held constant, the re-seeding rate increases as p_1 increases, with the minimum value occurring at 1000 Pa. According to Figure 21, it is inferred that as the negative pressure value increases, F_e of the seed metering disc on the seed population strengthens. When F_e exceeds the combined force of the interference between the seeds and the gravitational force of the seed population, a single pore may adhere to multiple seeds, leading to an increased re-seeding rate, consistent with bench test results.

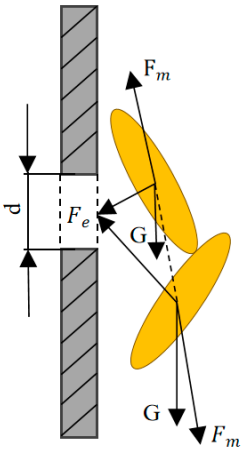

Figure 21. Schematic Diagram of Suction Force. F_e is the adsorption force of the seeding disc on the seed groups, N; F_m is the interference force between rice seeds, N.

With p_1 as a fixed parameter, the re-seeding rate slowly decreases as n_1 increases, reaching its minimum at 40 r/min. According to Newton's First Law, referring to a single pore, the centrifugal inertial force is proportional to the effective mass at that point and the square of the angular velocity. When a repeated seed suction occurs, the effective adhesive mass increases; as n_1 rises, the centrifugal inertial force significantly strengthens, preventing the seed adhesion force F_e from maintaining torque balance, causing excess seeds to detach, thereby reducing the re-seeding rate.

(3) Impact on Qualification Rate

When n_1 is held constant, the qualification rate initially increases and then decreases with increasing p_1, reaching a peak in the range of 1250 Pa to 1349 Pa. Conversely, when p_1 is fixed, the qualification rate also exhibits a pattern of first increasing and then decreasing as n_1 increases, peaking between 25.8 and 34.1 r/min. The primary reason for these trends is that the qualification rate is directly influenced by changes in the missed seeding rate

and re-seeding rate, as the sum of the probabilities of the qualification rate, missed seeding rate, and re-seeding rate equals 100%. Examination of the response surfaces for the missed seeding rate and re-seeding rate reveals that, within the p_1 range of 1250 Pa to 1349 Pa and n_1 range of 25.8 to 34.1 r/min, both rates approach their respective optimal values. Therefore, when p_1 and n_1 are each within their respective high-performance intervals, the qualification rate is maximized.

5. Conclusions

This study presents the design of a branched air-chamber type pneumatic seed metering device for rice. Through theoretical analysis, the minimum critical negative pressure required for the seed suction pores was clarified, and the branched air chamber casing impacting the device's seed suction performance was optimized via simulation tests. Additionally, bench tests were conducted to determine the optimal operational parameters. The main findings from the tests are summarized as follows:

(1) A force dynamics model for rice seeds was established to analyze the forces on seeds during the suction process by the metering device. A relationship between the negative pressure and diameter of the suction pores was derived, leading to a designed pore diameter of 1.44 mm. Based on this pore type, the minimum critical negative pressure required for stable seed adhesion was calculated to be 800 Pa.

(2) Using Ansys-Fluent software, a CFD domain single-factor and an L_9 (3^4) orthogonal test were conducted on the branched air chamber casing. The results showed that the maximum vacuum pressure in the seed metering disc pores was 857 Pa when the chamber depth was 22 mm, the chamber angle was 100°, and the chamber cavity depth was 25 mm, with the smallest coefficient of variation at 0.86%. Under these optimized conditions, a simulation verification test was conducted. The results indicated that the negative pressure at each suction pore was significantly higher than the minimum critical negative pressure of 800 Pa required for stable seed adhesion, thus confirming the optimized structure of the branched air chamber casing based on simulation results.

(3) Based on the branched air chamber casing design, and targeting seeding goals of 1–3, 2–4, and 5–8 seeds per hole, the bench tests used missed seeding rate, qualification rate, and re-seeding rate as test indices, with the number of openings, working negative pressure, and rotor speed as test factors. Single-factor test results identified the best number of openings as 2, 3, and 6, with an optimal working negative pressure range of 1000–1600 Pa, and an optimal rotor speed range of 20–40 r/min. Based on the regression orthogonal test results, the following conclusions were drawn: For seeding goals of 1–3 seeds per hole, the optimal operational parameters were a working negative pressure of 1355 Pa and a rotor speed of 32.78 r/min, resulting in a missed seeding rate of 4.70%, a qualification rate of 85.81%, and a re-seeding rate of 9.49%. For seeding goals of 2–4 seeds per hole, the optimal parameters were a working negative pressure of 1357 Pa and a rotor speed of 32.87 r/min, resulting in a missed seeding rate of 4.60%, a qualification rate of 85.59%, and a re-seeding rate of 9.81%. For seeding goals of 5–8 seeds per hole, the best parameters were a working negative pressure of 1339 Pa and a rotor speed of 31.07 r/min, with a missed seeding rate of 4.09%, a qualification rate of 87.27%, and a re-seeding rate of 8.64%. The study demonstrates that the seed metering device can effectively meet the varied direct seeding requirements of rice.

This research addresses the current academic gap by offering a pneumatic seed metering device capable of meeting the seeding requirements of super hybrid rice, common hybrid rice, and conventional rice. It enhances the adaptability of pneumatic rice seed metering devices to different seeding amounts and provides a reference for the optimized design of pneumatic seed metering devices.

Author Contributions: Conceptualization, X.Z. and L.C.; methodology, X.Z.; software, L.C.; validation, X.Z., L.C. and D.C.; formal analysis, X.Z.; investigation, X.Z., L.C., D.C., Y.H. and R.Y.; resources, R.Y.; data curation, D.C. and Y.H.; writing—original draft preparation, X.Z. and L.C.; writing—review and editing, X.Z. and L.C.; visualization, X.Z. and D.C.; supervision, R.Y.; project administration, R.Y.; funding acquisition, R.Y. All authors have read and agreed to the published version of the manuscript.

Funding: This work was financially supported by Hainan Provincial Natural Science Foundation (322QN233), Nanhai nova project in Hainan province (NHXXRCXM202308) and the National Key Research and Development Project of China (2023YFD2000400).

Institutional Review Board Statement: Not applicable.

Data Availability Statement: The data presented in this study are available on-demand from the second author at (22220951360007@hainanu.edu.cn). Data may be obtained from the College of Mechanical and Electrical Engineering, Hainan University, upon request and after authorization.

Acknowledgments: We thank Peiyu Wang for investigation assistance during the preparation of this manuscript. All supports and assistance are sincerely appreciated.

Conflicts of Interest: The authors declare no conflicts of interest.

References

1. Chhokar, R.S.; Sharma, R.K.; Gathala, M.K.; Pundir, A.K. Effects of crop establishment techniques on weeds and rice yield. *Crop Prot.* **2014**, *64*, 7–12. [CrossRef]
2. Mahajan, G.; Chauhan, B.S.; Gill, M.S. Dry-seeded rice culture in Punjab State of India: Lessons learned from farmers. *Field Crops Res.* **2013**, *144*, 89–99. [CrossRef]
3. Rao, A.N.; Brainard, D.C.; Kumar, V. Preventive weed management in direct-seeded rice: Targeting the weed seed bank. *Adv. Agron.* **2017**, *144*, 45–142.
4. Mishra, A.K.; Khanal, A.R.; Pede, V.O. Is direct seeded rice a boon for economic performance? Empirical evidence from India. *Food Policy* **2017**, *73*, 10–18. [CrossRef]
5. Kumar, V.; Laddha, J.K. Direct seeding of rice: Recent developments and future research needs. *Adv. Agron.* **2011**, *111*, 297–413.
6. Luo, X.; Wang, Z.; Zeng, S.; Zang, Y.; Yang, W.; Zhang, M. Recent advances in mechanized direct seeding technology for rice. *J. South China Agric. Univ.* **2019**, *40*, 1–13.
7. Zang, Y.; He, S.; Wang, Z.; Liu, S.; Wang, X.; Wen, Z. Design of pneumatic single seed metering device for coated hybrid rice. *Trans. CSAE* **2021**, *37*, 10–18.
8. Xing, H.; Wang, Z.; Luo, X.; Cao, X.; Liu, C.; Zang, Y. General structure design and field experiment of pneumatic rice direct-seeder. *J. Agric. Biol. Int. Eng.* **2017**, *10*, 31–42.
9. Xing, H.; Wang, Z.; Luo, X.; Zang, Y.; Yang, W.; Zhang, M.; Ma, Y. Design of an active seed throwing and cleaning unit for pneumatic rice seed metering device. *Int. J. Agric. Biol. Eng.* **2018**, *11*, 62–69. [CrossRef]
10. Zhang, M.; Wang, Z.; Luo, X.; Zang, Y.; Yang, W.; Xing, H.; Wang, B.; Dai, Y. Review of precision rice hill-drop drilling technology and machine for paddy. *Int. J. Agric. Biol. Eng.* **2018**, *11*, 1–11. [CrossRef]
11. Zheng, T.; Tang, X.; Luo, X.; Li, G.; Wang, Z.; Shu, S.; Chen, W. Effects of different irrigation methods on production of precision hill-direct-seeding super rice. *Trans. CSAE* **2010**, *26*, 52–55.
12. Zeng, X. The Research in Mechanization Planting Ways and Seeding Ratios at Different Early Direct Seeding Rice. Master's Thesis, Jiangxi Agricultural University, Nanchang, China, 2013.
13. Tang, H.; Xu, F.; Guan, T.; Xu, C.; Wang, J. Design and test of a pneumatic type of high-speed maize precision seed metering device. *Comput. Electron. Agric.* **2023**, *211*, 107997. [CrossRef]
14. Du, X.; Liu, C. Design and testing of the filing plate of inner-filling positive pressure high-speed seed -metering device for maize. *Biosyst. Eng.* **2023**, *228*, 1–17. [CrossRef]
15. Luo, X.; Liu, T.; Jing, E.; Li, Q. Design and experiment of hill sowing wheel of precision rice direct-seeder. *Trans. CSAE* **2007**, *23*, 108–112.
16. Tian, L.; Wang, J.; Tang, H.; Li, S.; Zhou, W.; Shen, H. Design and performance experiment of helix grooved rice seeding device. *Trans. Chin. Soc. Agric. Mach.* **2016**, *47*, 46–52.
17. Shi, S.; Liu, H.; Wei, G.; Zhou, J.; Jian, S.; Zhang, R. Optimization and experiment of pneumatic seed metering device with guided assistant filing based on EDEM-CFD. *Trans. Chin. Soc. Agric. Mach.* **2020**, *51*, 54–66.
18. Zhang, X.; Cheng, J.; Shi, Z.; Wang, M.; Fu, H.; Wu, H. Simulation and experiment of seed taking performance of swing-clamp type maize precision seed-metering device. *Trans. Chin. Soc. Agric. Mach.* **2023**, *54*, 38–50.
19. Wang, Z.; Huang, Y.; Wang, B.; Zang, M.; Ma, R.; Ke, R.; Luo, X. Design and experiment of rice precision metering device with sowing amountstepless adjusting. *Trans. CSAE* **2018**, *34*, 9–16.

20. Zang, Y.; Huang, Z.; Qin, W.; He, S.; Qian, C.; Jiang, Y.; Tao, W.; Zhang, M.; Wang, Z. Design of hybrid rice air-suction single seed metering device. *Trans. CSAE* **2024**, *40*, 181–191.
21. Xing, H.; Zang, Y.; Wang, Z.; Luo, X.; Zhang, M.; Fang, L. Design and experimental analysis of a stirring device for a pneumatic precision rice seed metering device. *Trans. ASABE* **2020**, *63*, 799–808. [CrossRef]
22. Xing, H.; Wang, Z.; Luo, X.; He, H.; Zang, Y. Mechanism modeling and experimental analysis of seed throwing with rice pneumatic seed metering device with adjustable seeding rate. *Comput. Electron. Agric.* **2020**, *178*, 105697. [CrossRef]
23. Zhang, G.; Zhang, S.; Yang, W.; Lu, K.; Lei, Z.; Yang, M. Design and experiment of double cavity side-filled precision hole seed metering device for rice. *Trans. CSAE* **2016**, *32*, 9–17.
24. Zhang, M.; Luo, X.; Wang, Z.; Dai, Y.; Wang, B.; Zheng, L. Design and experiment of combined hole-type metering device of rice hill-drop drilling machine. *Trans. Chin. Soc. Agric. Mach.* **2016**, *47*, 29–36.
25. Zhang, S.; He, H.; Yuan, Y.; Kang, F.; Xiong, W.; Li, Z.; Zhu, D. Design and experiment of the orifice-groove combined hole of the oriented filling type precision hill-drop seed-metering device for rice. *Trans. CSAE* **2023**, *39*, 39–50.
26. Xing, H.; Zhang, G.; Han, Y. Development and experiment of double cavity pneumatic rice precision direct seeder. *Trans. CSAE* **2020**, *36*, 29–37.
27. Luo, X.; Jiang, E.; Wang, Z.; Tang, X.; Li, J.; Chen, X. Precision rice hill-drop drilling machine. *Trans. CSAE* **2008**, *24*, 52–56.
28. Zhang, X. *Agricultural Machinery Design Manual*, 1st ed.; China Agricultural Science and Technology Press: Beijing, China, 2007; pp. 355–360.
29. Zhai, J. Design and Experiment of Pneumatic Precision Hill-Drop Drilling Seed Metering Device for Rice Budded Seed. Ph.D. Thesis, Huazhong Agricultural University, Wuhan, China, 2015.
30. Xing, H.; Zang, Y.; Wang, Z.; Zhang, G.; Cao, X.; Gu, X. Design and experiment of filling seed stratified room on rice pneumatic metering device. *Trans. CSAE* **2015**, *31*, 42–48.
31. Zha, X.; Zhang, G.; Han, Y.; Fu, J.; Zhou, Y. Design and optimization of centralized pneumatic fertilizer transporting system for deep fertilization device in paddy field. *Int. J. Fluid Mach. Syst.* **2021**, *14*, 309. [CrossRef]
32. Xing, H.; Zang, Y.; Wang, Z.; Luo, X.; Pei, J.; He, S.; Xu, P.; Liu, C. Design and parameter optimization of rice pneumatic seeding metering device with adjustable seeding rate. *Trans. CSAE* **2019**, *35*, 20–28.